Preemptive SOD1 Silencing via Neonatal Intramuscular AAV Therapy Modifies Disease Trajectory in an ALS Mouse Model

Xueqi Gong[1,2,3], Yecheng Xie[4], Wenyuan Wang[5,6*], Tonghui Xu[1,2,3*]
[1]Laboratory Animal Center, Fudan University, Shanghai, China.
[2]Laboratory Animal Resource Center, Fudan University, Shanghai, China.
[3]School of Life Sciences, Fudan University, Shanghai, China.
[4]Department of Neurology, Children's Hospital, Zhejiang, University School of Medicine, National Clinical Research, Center for Child Health, Hangzhou 310052, China
[5]Interdisciplinary Research Center on Biology and Chemistry, Shanghai Institute of Organic Chemistry, Chinese academy of Science, Shanghai, China.
[6]Department of Rehabilitation Medicine, Huashan Hospital, Fudan University, Shanghai, China.
*Corresponding authors: Tonghui Xu, Ph.D. Laboratory Animal Center, Fudan University, Shanghai, China. E-mail: xu_tonghui@fudan.edu.cn.
Wenyuan Wang, Ph.D. Interdisciplinary Research Center on Biology and Chemistry, Shanghai Institute of Organic Chemistry, Chinese academy of Science, Shanghai 200032, China. E-mail: wywang@sioc.ac.cn.

Abstract

Amyotrophic lateral sclerosis (ALS) is a fatal neurodegenerative disorder with limited treatment options. Mutations in *SOD1* are a leading genetic cause of familial ALS, driving motor neuron degeneration through toxic gain-of-function mechanisms. While gene silencing strategies targeting *SOD1* hold therapeutic promise, their clinical translation has been hindered by inefficient delivery to the spinal cord and safety concerns associated with conventional viral vectors. Here, we report a minimally invasive gene therapy strategy that combines the retrograde transport capability of rAAV2-retro with the safety of an artificial microRNA (miRNA) to achieve pan-spinal SOD1 suppression. A single intramuscular injection of rAAV2-retro-miRNA into neonatal *SOD1*^{G93A} mice resulted in widespread transduction of spinal motor neurons, significant reduction of mutant SOD1 protein, and multifaceted therapeutic benefits. Treated mice exhibited delayed disease onset, extended survival, preserved motor function, reduced neuroinflammation, and protection of neuromuscular junctions and spinal motor neurons. Importantly, the artificial miRNA platform demonstrated a superior safety profile compared to shRNA-based constructs, which caused severe toxicity and lethality in wild-type mice. Our study establishes neonatal intramuscular delivery of rAAV2-retro-miRNA as a safe, efficient, and clinically translatable

strategy for preemptive intervention in *SOD1*-mediated ALS, with broad implications for the treatment of other motor neuron diseases.

Introduction

Amyotrophic lateral sclerosis (ALS) is a fatal neurodegenerative disease characterized by the progressive destruction of both upper motor neurons in the cerebral cortex and lower motor neurons in the brainstem and spinal cord[1]. Despite significant research efforts, the precise cause or etiology of ALS remains unknown. This incurable disease is marked by the insidious onset of paralysis, respiratory failure, and fatal decline within 2-5 years of symptom presentation. The pathophysiology of ALS involves multiple interconnected mechanisms, including disrupted RNA-protein balance, perturbed transport between nucleo-cytoplasmic and axonal compartments, mitochondrial dysfunction coupled with oxidative stress, excitotoxic pathways, and neuroinflammation [2] Due to the absence of identified therapeutic targets, current management strategies focus on symptom relief and respiratory support[3,4]. Currently available small-molecule medications, such as riluzole, edaravone (Radicava), and sodium phenylbutyrate-taurursodiol, aim to modulate glutamatergic transmission or alleviate oxidative stress but have shown only modest therapeutic effects in clinical trials [4-6].

Approximately 10% of ALS cases are familial, reflecting a significant genetic component, and known gene mutations account for about 70% of these familial cases[7]. Known mutations, predominantly in genes encoding superoxide dismutase 1 (*SOD1*)[8], TAR DNA-binding protein 43 (*TDP-43*), [9,10] fused in sarcoma (FUS), [11,12] and the C9ORF72 hexanucleotide repeat expansion,[13,14] account for the majority of familial ALS. Among these, *SOD1* mutations represent one of the earliest identified and most extensively studied genetic causes.[8,15-17] Recently, tofersen, an FDA-approved antisense oligonucleotide (ASO) targeting SOD1, achieved up to 36% reduction in CSF SOD1 concentration at the highest dose,[18,19] demonstrating the feasibility of gene-targeting therapies for ALS. While the generality of its clinical effects requires further validation due to the current small sample size,[18] this milestone approval validates the therapeutic strategy for ALS. In this context, gene therapy has emerged as a transformative new hope for treating ALS, aiming to deliver functional genes, neuroprotective factors, or agents to silence the expression of pathogenic gene.

In the realm of gene therapy for neurodegenerative diseases such as ALS, adeno-associated virus (AAV) vectors have emerged as pivotal delivery vehicles due to their proven safety profile, minimal immunogenicity, and ability to sustain long-term transgene expression across diverse central nervous system cell populations.[20,21] This inherent delivery advantage directly enables the precise implementation of gene silencing strategies—therapeutic approaches that selectively suppress disease-causing mutations at their genetic source. In the gene therapy for ALS, AAV's capability to efficiently transduce neural cells makes it particularly well-suited for delivering silencing constructs targeting mutant forms of cytosolic superoxide dismutase (SOD1), a well-established genetic driver of ALS pathogenesis and a major focus of therapeutic development.[8,15-17] To achieve this targeted silencing, researchers increasingly utilize small noncoding RNAs as therapeutic effectors, with short hairpin RNAs (shRNAs)

and artificial microRNAs (miRNAs) representing the most promising molecular tools. While both RNA species mediate potent gene suppression, artificial miRNAs demonstrate particular advantages through their enhanced biosafety profile, making them especially valuable for chronic neurodegenerative indications such as ALS where sustained therapeutic effects are required.[22,23]

However, achieving efficient and sustained therapeutic gene delivery to affected neural compartments—particularly spinal motor neurons across lumbar, thoracic, and cervical segments—remains a fundamental challenge in ALS gene therapy. Current delivery modalities, including intracerebroventricular (ICV), intrathecal (IT), spinal subpial, and intraparenchymal injections face significant translational limitations: These invasive neurosurgical procedures require specialized instrumentation, carry inherent procedural risks, and present substantial clinical safety concerns. While intramuscular (IM) injection offers compelling advantages in simplicity and reduced invasiveness, prior studies administering AAV-encoded neuroprotective factors (e.g., IGF1, IGF2, HGF) via IM routes have demonstrated only modest therapeutic efficacy in *SOD1* ^{G93A} models, which may relate to due to suboptimal transduction efficiency of spinal motor neurons.[24-28] Critically, direct mutant SOD1 silencing via this route remains unexplored and lacks therapeutic validation. Consequently, advancing clinically viable ALS gene therapies necessitates strategies that reconcile broad neuraxial distribution with minimally invasive administration and low vector doses.

To address these delivery limitations, we developed a novel gene silencing strategy utilizing rAAV2-retro vectors administered via intramuscular (IM) injection in the *SOD1* ^{G93A} transgenic mouse model of ALS. Our prior work demonstrated that a single IM injection of rAAV2-retro into neonatal mice achieves extensive transduction of motor neurons throughout the spinal cord and brainstem nuclei, offering three critical advantages for motor neuron disease therapy: (1) highly efficient retrograde transduction of lower motor neurons; (2) minimally invasive peripheral delivery; and (3) preferential tropism for motor neurons, minimizing off-target effects.[29] Based on this highly efficient delivery platform, we hypothesized that a single neonatal IM injection of rAAV2-retro encoding an artificial miRNA could achieve pan-spinal SOD1 silencing, thereby delaying disease onset and prolonging survival in *SOD1* ^{G93A} mice**.** The *SOD1* ^{G93A} model—which ubiquitously expresses mutant human SOD1 protein[30]—recapitulates core ALS pathophysiology including progressive motor neuron loss, paralysis, and premature death, making it an ideal model to test this hypothesis. In this study, we demonstrate that this strategy indeed enables widespread spinal cord transduction and robust SOD1 suppression, which significantly delays disease onset, preserves motor function, attenuates neuropathology, and extendes survival. By overcoming traditional CNS delivery barriers through a simple peripheral route, our approach addresses a critical unmet need in ALS gene therapy and provides a clinically translatable platform for targeted silencing strategies.

Methods

Animals

C57BL/6J (stock no.000664) mice and high-copy transgenic *SOD1* ^{G93A} mice [B6. Cg-Tg(*SOD1*^{G93A})/1Gur/J] (stock no.004435) were purchased from the Jackson Laboratory. Transgenic littermates of both sexes expressing high levels of the mutant *SOD1* ^{G93A} transgene were randomly and equally allocated to experimental groups, while non-transgenic littermates served as controls. All animals were housed under specific pathogen-free (SPF) conditions with controlled temperature, humidity, light, and noise. Mice were maintained on a 12-hour light/dark cycle with ad libitum access to food and water in the institutional animal care facility. All procedures involving mice were approved by the Animal Experimental Ethics Committee of Shanghai Medical School, Fudan University, China and conducted in compliance with its institutional guidelines.

Production, Purification, and Titration of Recombinant AAV Vectors

A single-stranded recombinant AAV2-retro vector was designed to express enhanced green fluorescent protein (eGFP) under the control of a CAG promoter. The construct also includes a synthetic microRNA (miRNA) targeting human SOD1 mRNA(exon 2), followed by the woodchuck hepatitis virus post-transcriptional regulatory element (WPRE) and an SV40 polyadenylation signal. The artificial miRNA, designed to silence human SOD1 without affecting mouse SOD1, was embedded within the human miR-30a scaffold as previously described. The complete oligonucleotide sequence of the artificial miRNA is provided below, with the guide strand underlined: miR-30a construct:5'-TGTTTGAATGAGGCTTCAGTACTTTACAGAATCGTTGCC TGCACATCTTGGAAACACTTGCTGGGATTACTTCTTCAGGTTAACCCAACAGAAGGCA AAGAAGGTATATTGCTGTTGACAGTGAGCG<u>TCATGAACATGGAATCCATG</u>TAGTGAAG CCACAGATGTAAAGGTGGATGAAGAAAGTATGCCTACTGCCTCGGACTTCAAGGGGCT ACTTTAGGAGCAATTATCTTGTTTACTAAAACTGAATACCTTGCTATCTCTTTGATACATT TTTACAAAGCTGAATTAAAATGGTATAAATTAAATCACTTTA-3'.

The recombinant vectors were packaged into AAV2 capsids via triple plasmid transfection of HEK 293 cells. The transfection mixture included: (1) the AAV2 inverted terminal repeat (ITR)-based transgene plasmid, (2) a helper plasmid expressing AAV2 Rep and Cap genes, and (3) the adenoviral helper plasmid pHELP. Subsequently, viral particles were purified and titers were determined using quantitative PCR (qPCR).

Similarly, the rAAV2-retro-shRNA vector was engineered to express a short hairpin RNA (shRNA) targeting human SOD1 mRNA (exon 2) under the control of the CAG promoter, followed by an SV40 polyadenylation signal.

Intramuscular injection

As previously described, cryoanesthesia was induced in postnatal day 4 (P4) mice using pre-chilled aluminum plates.[29] For intramuscular injections, fine surgical scissors were used to make small incisions over the left forelimb and right hindlimb of the neonatal mice to expose the flexor carpi ulnaris and gastrocnemius muscles, respectively. All viral vectors were diluted in phosphate-buffered saline (PBS) to a concentration of 1×10^{13} genomic copies (GC)/mL. A total volume of 2 μL, containing 2×10^{1}□ GC of each vector, was injected into the left flexor carpi ulnaris and right gastrocnemius muscles. Injections were performed using a glass micropipette

connected to a high-precision syringe pump (Quintessential Stereo taxic Injector, Model 53311) at a constant rate of 1.0 μL/min. The pipette was held in place for 30 seconds after injection before being slowly withdrawn to minimize reflux and prevent viral leakage.

Western blot

Mice under deep anesthesia were decapitated and tissues were quickly dissected, snap-frozen in liquid nitrogen, and stored at -80□. For protein extraction, frozen tissues or cultured cells were homogenized in RIPA buffer (Beyotime, P0013B) supplemented with a protease inhibitor cocktail (Beyotime, ST506). Subsequently, samples were mixed with loading buffer (Tsingke, TSJ010) and heated at 100□°C for 10 minutes. Proteins were separated by SDS-PAGE and transferred onto polyvinylidene fluoride (PVDF) membranes. The membranes were blocked with 5% non-fat dry milk in Tris-buffered saline containing 0.05% Tween-20 (TBST; 20 mM Tris-HCl, 150 mM NaCl, pH 7.5) for 1 hour at room temperature, followed by incubation with primary antibodies overnight at 4□°C. After washing, the membranes were incubated with horseradish peroxidase (HRP)-conjugated secondary antibodies. The following primary and secondary antibodies were used: mouse anti-hSOD1 (1:200, Santa Cruz Biotechnology, sc-17767), mouse anti-Actin (1:5000, Proteintech, 66009-1-IG), mouse anti-eGFP (1:1000, Santa Cruz Biotechnology, sc-5384), and HRP-conjugated goat anti-mouse IgG (1:5000, YEASEN, 33201ES60). Protein bands were visualized using enhanced chemiluminescence, and band intensities were quantified using Image Lab (Bio-Rad) or ImageJ software, normalized to the loading control in each lane.

RNA Extraction, Reverse Transcription, and Quantitative Real-Time PCR

Total RNA was extracted from cultured N2A cells using TRIzol™ Reagent (Thermo Fisher Scientific, 15596018CN) according to the manufacturer's protocol. RNA concentration and purity were assessed spectrophotometrically by measuring the absorbance at 260 nm and calculating the 260/280 nm ratio. Complementary DNA (cDNA) was synthesized from 1 μg of total RNA using random primers and the Hifair® III First Strand cDNA Synthesis Kit (Yeasen Biotechnology, 11141ES60).

Quantitative real-time PCR (qPCR) was performed using the 2× SYBR Green qPCR Master Mix (Selleck Chemicals, B21203) on a Bio-Rad iCycler iQ6 detection system. Each reaction contained cDNA derived from 100 ng of total RNA. The amplification conditions followed the manufacturer’s instructions. The human *SOD1* gene was amplified with the following primers:

Forward: 5′-GGGAAGCTGTTGTCCCAAG-3′

Reverse: 5′-CAAGGGGAGGTTAAAAGAGAGC-3′

Mouse GAPDH (NM_001289726.2) was used as an endogenous control and amplified with the primers:

Forward: 5′-CACCATCTTCCAGGAGCGAG-3′

Reverse: 5′-CCTTCTCCATGGTGGTGAAGAC-3′

Data were collected and analyzed using the Bio-Rad iQ6 optical system software.

Behavior analysis

Body weight measurement: Weekly monitoring of body weight was performed for WT, rAAV2-retro-Scramble-treated and rAAV2-retro-miRNA-treated ALS mice.

Rotarod test: Mice were subjected to weekly rotarod testing consisting of three trials per session. The rotarod accelerated from 5 rpm to 40 rpm per minute (KEW BASIS, KW-6D). The latency to fall was recorded for each mouse.

Limb clasping assay: Hindlimb clasping behavior was assessed at 135 days of age by suspending

mice by the tail for 10 seconds with their heads oriented downward. A clasping score was assigned if the behavior persisted for more than 2 seconds according to the following criteria: 1 point for clasping in one hindlimb, 2 points for clasping in both hindlimbs, and 3 points if clasping involved hindlimbs, forelimbs, and torso.

Grip-strength test: Forelimb and hindlimb grip strength was measured using a grip-strength meter (KEW BASIS, KW-ZL). Mice were positioned such that only the forelimbs or hindlimbs could grasp the bar. Each mouse was gently pulled backward with a consistent force until the bar was released. The peak tension (in grams) was recorded over five consecutive trials.

Open-field test: Locomotor activity was evaluated by allowing mice to move freely for 1 hour in a clean, opaque acrylic open-field arena (50 cm × 50 cm). Movement was tracked using EthoVision Video Tracking Software (Noldus), and the total distance traveled was analyzed.

Assessment of Disease Progression and Survival

The endpoint was defined as the humane experimental endpoint, corresponding to the time at which the animal could no longer right itself within 30 seconds after being placed on its back. Disease onset and progression were evaluated through retrospective analysis of the collected data. Disease onset was defined as the age at which the animal attained its peak body weight. The overall disease duration was calculated as the interval between disease onset and the endpoint. The early disease phase was designated as the period from peak weight to a 10% loss of peak body weight, while the late disease phase was defined as the period from 10% weight loss to the endpoint.

Compound Muscle Action Potential (CAMP) Measurement

At 130 days of age, mice were anesthetized with isoflurane, and hair was removed from the hindlimb and lower back regions using depilatory cream prior to recording. The stimulating electrode was placed at the lumbar spinal roots, while the active recording electrode was positioned over the belly of the gastrocnemius muscle. The reference electrode was placed near the Achilles tendon or digit of the ipsilateral hindlimb (iWork, IX-RA-834ECG).

Tissue preparation

Following euthanasia via isoflurane overdose, mice were transcardially perfused with phosphate-buffered saline (PBS), followed by 4% paraformaldehyde (PFA) in PBS. The perfused tissues were then post-fixed in 4% PFA overnight at 4□°C. The spinal cords were dehydrated in 30% sucrose for 24 hours and sectioned at a thickness of 30 μm using a freezing microtome (Leica, CM3050 S). Gastrocnemius muscle and liver tissues were dehydrated, embedded in paraffin, and sectioned into 3 μm-thick slices with a rotary microtome (Leica, 149BIO000C1).

Immunohistochemistry

For immunohistochemical staining of spinal cord sections, fixed tissues were washed three times with PBS and subjected to antigen retrieval using 1× citrate buffer (Sangon Biotech, A100101-0500). Sections were then blocked with 5% goat serum (Sangon Biotech, E510009-0100) and 0.3% Triton X-100 (Beyotime, P0096) in PBS for 1 hour at room temperature. After blocking, the slices were incubated with primary antibodies diluted with 3% goat serum (Sangon Biotech, E510009-0100) and 0.1% Triton X-100 (Beyotime, P0096) in PBS at 4°C overnight. The following primary antibodies were used: rabbit anti-ChAT (1:1000, Abcam, ab178850), chicken anti-NeuN (1:1000, Millipore, ABN91), mouse anti-eGFP (1:1000, Santa Cruz Biotechnology, sc-5384), rabbit anti-Iba1 (1:1000, Abcam, ab178846), rabbit anti-GFAP (1:1000, Abcam, ab7260), rabbit anti-hSOD1 (1:500, Cell Signaling Technology, 2770). After incubation, sections were

washed three times with PBS and incubated with corresponding secondary antibodies for 2 hours at room temperature in the dark. Secondary antibodies included: donkey anti-mouse Alexa Fluor 488 (1:500, Thermo Fisher, A-20102), goat anti-chicken Alexa Fluor 647 (1:1000, Abcam, ab150171), donkey anti-rabbit Alexa Fluor 555 (1:500, Thermo Fisher, A-31572). nuclei were counterstained with DAPI (1:1000, Sigma-Aldrich, 10236276001) in PBS for 10 minutes, followed by three PBS washes. Finally, sections were mounted with an antifade mounting medium (SouthernBiotech, 0100-01) for imaging.

For immunohistochemical staining of liver sections, paraffin-embedded slides were deparaffinized in xylene (Sinopharm Chemical Reagent, 10023428) and rehydrated through a graded ethanol series (Sinopharm Chemical Reagent, 100092680). Antigen retrieval was performed using microwave heating in Tris-EDTA buffer (Solarbio, C1038). Sections were then blocked with 5% normal goat serum for 1 hour at room temperature and incubated overnight at 4°C with the following primary antibody: mouse anti-eGFP (1:1000, Santa Cruz Biotechnology, sc-5384). After washing three times with TBS-T, slides were incubated with the corresponding secondary antibody for 1–2 hours at room temperature in the dark: donkey anti-mouse Alexa Fluor 488 (1:500, Thermo Fisher, A-20102). Nuclei were stained with DAPI (1:1000, Sigma-Aldrich, 10236276001) for 10 minutes, followed by washing with TBS-T. Finally, sections were mounted using antifade mounting medium (SouthernBiotech, 0100-01) for subsequent imaging.

For immunostaining of NMJs, gastrocnemius muscles were dissected and teased into small bundles comprising two to three muscle fibers as previously described.[31] Tissues were then immunostained using chicken anti-neurofilament (1:2500, Abcam, ab4680) to label presynaptic axons and fluorophore-conjugated α-bungarotoxin (α-BTX, Biotium, 00018) to identify postsynaptic acetylcholine receptors.

For H&E Staining of muscle sections, gastrocnemius tissue sections were deparaffinized in xylene (Sinopharm Chemical Reagent, 10023428) and rehydrated through a graded ethanol series (Sinopharm Chemical Reagent, 100092680). Nuclei were stained with Harris hematoxylin (Beyotime, C0107) for 5 minutes, followed by rinsing under tap water and differentiation in 1% acid alcohol (Beyotime, C0163M). Sections were then blued in Scott's tap water substitute and rinsed. Cytoplasmic counterstaining was performed using eosin (Beyotime, C0109) for 1 minute. After dehydration through a graded ethanol series and clearing in xylene, the sections were mounted with a resinous medium (Sangon, E675007).

Fluorescence microscopy

Spinal cord and liver tissue sections were initially scanned using a digital slide scanner (PANNORAMIC 250 Flash III, 3DHISTECH) equipped with a 20× objective lens. High-magnification representative images were acquired with a Leica SP8 confocal microscope using a 40× oil-immersion objective. High-resolution z-stack images were obtained comprising 10–15 optical sections with step sizes of 0.3 μm (liver slices) or 4 μm (spinal cord slices). For neuromuscular junctions (NMJs), imaging was performed on an Olympus spin SR confocal microscope with a 20× objective, and maximum-intensity projections were generated using Fiji software for enhanced visualization. Additionally, hematoxylin and eosin (H&E)-stained sections of gastrocnemius muscle were digitized using the PANNORAMIC 250 Flash III slide scanner with a 10× objective.

Motoneuron quantification

Motoneurons were quantified using QuPath and Imaris software. TIFF images were first imported

into QuPath, where regions of interest (ROIs) were manually annotated. Nuclei within these ROIs were identified in the DAPI channel using the built-in “cell detection” function to generate initial detection outputs. These detections were further classified with the “Classify” tool, wherein detection parameters were optimized to reliably identify ChAT-positive and NeuN-positive cells. The resulting classifications were subsequently validated through manual verification performed in Fiji to ensure counting accuracy.

Quantification of Glial and Human SOD1 Signal Intensity

Fluorescence intensity was quantified using ImageJ software. The analysis procedure involved importing microscopy images into ImageJ and converting them to 8-bit format. Multi-channel datasets were deconvolved into individual channels to isolate specific fluorescent signals. Regions of interest (ROIs) were delineated based on fluorescence distribution. Thresholds were then carefully adjusted relative to background intensity to enhance measurement accuracy. The "Area" and "Integrated Density" within these ROIs were measured to obtain quantitative values for fluorescence intensity.

Quantification of Neuromuscular Junctions (NMJs)

Z-stack images of NMJs were acquired and processed using ImageJ as previously described. Endplates were classified as innervated if they exhibited co-localization of BTX and NF signals. Conversely, endplates showing only BTX staining without associated NF signal were classified as denervated.

Cross-sectional area (CSA) of muscle

The Fiji software was used to automatically identified the CSA of the gastrocnemius muscle, followed by manual correction to ensure accuracy. The CSA of individual fibers was then quantified using the “Analyze Particles” function. For each mouse, at least 1000 muscle fibers were assessed, and values were averaged.

Statistical analyses

Data that followed a normal distribution were analyzed using the unpaired Student’s t-test for comparisons between two groups. For comparisons among multiple groups or across time points, ANOVA was applied as appropriate. Survival data were analyzed using the Kaplan–Meier method, and group comparisons were made with the log-rank test. Normally distributed continuous data are presented as mean ± standard deviation (SD). Significance levels were defined as follows: $P < 0.05$, $*P < 0.01$, $**P < 0.001$, and $***P < 0.0001$. The number of replicates per experiment is indicated in the respective figure legends. All statistical analyses were conducted using GraphPad Prism 7 (GraphPad Software, San Diego, CA, USA).

Results

rAAV2-retro-mediated delivery of an artificial miRNA targeting human SOD1 achieves efficient spinal cord transduction and robust gene silencing in *SOD1* ^{G93A} mice

To develop a novel gene therapy strategy for amyotrophic lateral sclerosis (ALS), we investigated whether an artificial miRNA targeting human SOD1 could be delivered to the spinal cord via intramuscular (IM) injection of rAAV2-retro in *SOD1* ^{G93A} mice. This approach leverages the robust retrograde transport capability of rAAV2-retro to transduce spinal motor neurons from the muscle, offering a minimally invasive route for targeting the central nervous system (CNS) [29]. To

this end, we designed an artificial miRNA based on the human miR-30a scaffold as previously described,[32] which exhibits perfect complementarity to human SOD1 mRNA but contains at least four base mismatches with the murine SOD1 sequence to ensure species-specific silencing (Figure 1A). This miRNA expression cassette, along with an eGFP reporter gene, was cloned into the rAAV2-retro vector under the control of a CAG promoter (designated rAAV2-retro-miRNA). A control vector expressing a scrambled miRNA sequence (rAAV2-retro-Scramble) was also generated.

To evaluate the silencing efficacy of the constructed miRNA, *SOD1* ^{G93A} mice (n = 4) received bilateral intramuscular co-injections of rAAV2-retro-miRNA into the extensor carpi radialis (forelimb) and gastrocnemius (hindlimb) muscles at postnatal day 4 (P4; 1 µL per site, 1.0×10^{13} GC/mL). Four weeks post-injection, Western blot analysis of lumbar spinal cord lysates revealed a significant reduction (47.2%) in human SOD1 protein levels compared to rAAV2-retro-Scramble-treated animals (Figures 1B and 1C). Importantly, the artificial miRNA did not significantly alter the expression of endogenous murine SOD1 mRNA (Figure S1), confirming its specificity for the human transgene.
Motivated by this promising knockdown results, we proceeded to evaluate the therapeutic potential of this strategy. *SOD1* ^{G93A} mice of both sexes were treated at P4 with intramuscular injections of either rAAV2-retro-miRNA or rAAV2-retro-Scramble (1 µL per muscle, 1.0×10^{13} GC/mL). A comprehensive set of functional and behavioral assays was performed longitudinally, including assessment of disease onset (defined by peak body weight decline), survival, motor performance (rotarod, grip strength, open-field tests), and neurological signs (limb clasping). Terminal electrophysiological (CMAP) and histological analyses were conducted at 130 days of age (Figure 1D).

Having established the efficacy and specificity of our gene silencing platform, we compared its safety profile to that of a conventional shRNA approach in wild-type mice. Neonatal mice received intramuscular injections of either rAAV2-retro-miRNA or rAAV2-retro-shRNA at P4. Strikingly, while the artificial miRNA construct had no adverse effects on body weight or survival, delivery of the shRNA construct induced significant weight loss within one week and uniform lethality by three weeks post-injection (Figure S2). This dramatic difference underscores the superior safety profile of the artificial miRNA platform, a crucial advantage for therapeutic applications in the CNS.

Intramuscular delivery of rAAV2-retro-miRNA significantly delays disease onset and extends survival in *SOD1*^{G93A} mice

To evaluate the therapeutic potential of rAAV2-retro-mediated SOD1 silencing, we longitudinally monitored disease progression in treated *SOD1*^{G93A} mice by measuring body weight and survival until the humane endpoint (Figure S3). Disease onset was defined as the age at which animals sustained a 10% loss from their peak body weight. Remarkably, rAAV2-retro-miRNA treatment significantly delayed disease onset by 38 days compared to scramble-injected controls (median onset: 171.5 vs. 133.5 days; $P < 0.0001$; Figure 2A). Moreover, miRNA-treated mice exhibited a pronounced extension in median survival, living 61 days longer than scramble-injected control

animals (median survival: 216 days vs. 155 days; $P < 0.0001$; Figure 2B, C). Further analysis of disease phases revealed that the early disease period—from peak weight to 10% weight loss—was significantly prolonged in miRNA-treated mice (67.08 days vs. 49.00 days in controls; $P = 0.0188$; Figure 2D). The late disease phase, from 10% weight loss to end-stage, was also significantly lengthened (25.67 days vs. 16.33 days; $P = 0.0351$; Figure 2E). Consequently, the total disease duration was substantially longer in the rAAV2-retro-miRNA group (92.75 days) relative to the scramble control group (65.33 days; $P = 0.0005$; Figure 2F). These results demonstrate that a single neonatal intramuscular injection of rAAV2-retro-miRNA profoundly delays disease progression and improves survival in this ALS model.

Intramuscular delivery of rAAV2-retro-miRNA preserves motor function in *SOD1*^{G93A} mice

To comprehensively evaluate neuromuscular integrity, we performed a longitudinal behavioral battery starting at postnatal day 60, including rotarod, grip strength, open-field, and limb clasping assays—all conducted by investigators blinded to the treatment groups. rAAV2-retro-miRNA treatment conferred robust preservation of motor function. By 18 weeks, open-field locomotion had declined by only 33.9% in miRNA-treated mice, compared to a 75.74% reduction in scramble controls (Figure 3A). Strikingly, at 135 days, all scramble-treated mice exhibited dystonic clasping, whereas one-third of miRNA-treated animals remained completely free of this neurological sign (Figure 3B). Furthermore, miRNA-treated mice demonstrated significantly enhanced motor coordination on the rotarod, as well as greater forelimb and hindlimb grip strength compared to scramble controls (Figures 3C, D), indicating sustained preservation of motor function and muscle strength throughout their extended survival.

rAAV2-retro-miRNA gene therapy mitigates neuromuscular junction denervation and muscle atrophy in *SOD1*G93A mice

We next assessed the protective effects of rAAV2-retro-miRNA on the integrity of neuromuscular junction (NMJ) and muscle morphology. Consistent with the progressive nature of ALS, only 10.12% of NMJs remained fully innervated in scramble-treated *SOD1*^{G93A} mice at day 130, with the majority being partially or fully denervated (Figures 4A, B). In contrast, neonatal treatment with rAAV2-retro-miRNA significantly preserved NMJ innervation and reduced denervation.
Given the critical role of NMJ integrity in maintaining muscle mass, we quantified myofiber cross-sectional area (CSA) based on laminin staining. Scramble-treated *SOD1*^{G93A} mice exhibited severe muscle atrophy, with a mean CSA (765.7 μm^2) significantly smaller than that of wild-type mice (3009 μm^2; $P = 0.0008$; Figures 4C, D). rAAV2-retro-miRNA treatment markedly attenuated this atrophy, increasing mean CSA to 2090 μm^2 ($P = 0.0038$ vs. scramble; Figures 4C, D), and prevented the loss of whole-muscle mass (Figure S4).

To functionally evaluate NMJ transmission, we measured compound muscle action potential (CMAP) amplitudes at 130 days. rAAV2-retro-miRNA-treated mice showed significantly higher CMAP amplitudes compared to scramble controls (Figures 4E, F), indicating improved neuromuscular transmission and delayed functional denervation. Collectively, these results demonstrate that rAAV2-retro-miRNA therapy effectively preserves NMJ innervation, alleviates

muscle atrophy, and maintains electrophysiological function in *SOD1*^{G93A} mice.

Intramuscular delivery of rAAV2-retro-miRNA preserves spinal α-motoneurons and suppresses mutant SOD1 expression in *SOD1*^{G93A} mice

The degeneration of motor neurons and skeletal muscle denervation are hallmark pathological features of ALS. Immunohistochemical analysis revealed severe loss of α-motoneurons across all spinal cord segments in scramble-treated *SOD1*^{G93A} mice at day 130, compared to wild-type controls. In contrast, treatment with rAAV2-retro-miRNA significantly preserved α-motoneuron survival throughout the spinal cord (Figures 5A, B). Furthermore, whereas scramble-treated *SOD1*^{G93A} mice exhibited a decline in NeuN□ neurons to roughly 50% of wild-type levels (cervical: 55.44%; thoracic:57.44 %; lumbar: 48.94%), those treated with rAAV2-retro-miRNA retained over 70% of NeuN□ neurons (cervical: 76.16%; thoracic: 74.49%; lumbar: 70.32%). Concordant with these neuroprotective effects, robust human SOD1 (hSOD1) immunoreactivity was observed in the spinal cord of scramble-treated *SOD1*^{G93A} mice, whereas rAAV2-retro-miRNA treatment markedly suppressed hSOD1 expression (Figures 5C, D). These results demonstrate that neonatal intramuscular delivery of rAAV2-retro-miRNA effectively reduces mutant SOD1 levels and confers broad neuroprotection within the spinal cord.

Intramuscular delivery of rAAV2-retro-miRNA attenuates neuroinflammation in the spinal cord of *SOD1*^{G93A} mice

Neuroinflammation, marked by microglial and astrocytic activation, represents a key pathological hallmark of ALS. We therefore assessed whether rAAV2-retro-miRNA treatment could mitigate neuroinflammatory responses in the spinal cord. Immunofluorescence analysis revealed a significant reduction in the intensity of Iba1 (microglia) and GFAP (astrocytes) signals in rAAV2-retro-miRNA-treated mice compared to scramble-injected *SOD1*^{G93A} controls (Figure 6), indicating suppressed activation of both microglia and astrocytes. These results demonstrate that targeted suppression of mutant SOD1 via rAAV2-retro-miRNA not only protects motor neurons but also attenuates neuroinflammation in this ALS model.

Discussion

In this study, we established a novel and minimally invasive gene therapy strategy that combines the superior retrograde transport capability of rAAV2-retro with the safety profile of an artificial miRNA to achieve targeted silencing of the human SOD1 gene. A single intramuscular injection administered to neonatal *SOD1*^{G93A} mice resulted in widespread transgene expression across the spinal cord, a significant reduction of mutant SOD1 protein, and a multifaceted therapeutic benefit that included delayed disease onset, extended survival, preserved motor function, and protection of neuromuscular junctions and spinal motor neurons. Our strategy overcomes critical delivery barriers associated with conventional

CNS-directed gene therapies, providing a novel foundation for preemptive intervention in inherited ALS. This study demonstrates significant technological improvements through the following strategies: First, the use of rAAV2-retro, a vector with superior retrograde transduction efficiency in newborn animals, overcomes the low spinal cord transduction rates of traditional AAV serotypes in adult animals. Neonatal intramuscular injection of rAAV2-retro-CAG-miRNA achieved high-coverage gene silencing in motor neuron population across the entire spinal cord, surpassing the localized transduction limitations of prior studies (2020-rAAV2-Retro Enables Extensive and High-Efficient Transduction of Lower Motor Neurons following Intramuscular Injection). Second, unlike single neurotrophic factor delivery, this study employs miRNA-mediated *SOD1* gene silencing to block toxic protein aggregation and its downstream molecular cascades (e.g., mitochondrial dysfunction, neuroinflammation) at the source. This "upstream interception" strategy addresses the core pathology of ALS, contrasting with growth factor therapies that merely support neuronal survival. Third, capitalizing on neonatal immune immaturity and rAAV2-retro's genomic persistence, a single intramuscular injection establishes a durable therapeutic foundation that sustains efficacy throughout maturation, significantly reducing intervention burden in adulthood. Compared to the limitations of adult interventions requiring high doses or invasive procedures due to mature BBB and heightened immune surveillance, this early intervention serves as a foundational therapy with unique translational advantages.

This study pioneers a developmental early intervention strategy, achieving for the first time pan-spinal precision-targeted *SOD1* gene silencing in presymptomatic *SOD1*^{G93A} neonatal mice. This successfully disrupted the vicious cycle between neuroinflammation and neuromuscular junction degeneration, significantly delaying ALS pathological progression and extending the lifespan of ALS mice. Our finding aligns with the seminal AAV10-U7 study[33] where combined intracerebroventricular and intravenous (i.c.v./i.v.) injection at postnatal day 1 strikingly extended median survival, validating the critical therapeutic window for presymptomatic intervention in *SOD1*-mediated ALS. These findings carry substantial scientific and clinical implications: First, SO*D1* mutation, as a core genetic etiology of familial ALS, initiates pathological effects as early as the embryonic stage.[34] Critically, *SOD1*^{G93A} mice exhibit subclinical pathology (e.g., motor neuron hyperexcitability) shortly after birth, yet early pathogenic processes are masked by compensatory mechanisms that delay overt symptoms for months[17]. Our strategy intervenes before the potential age-dependent failure of compensation and the theoretical point-of-no-return for neurodegeneration—thereby, maximizing the benefit of SOD1 silencing by halting toxicity at its origin. Second, we demonstrate that during the neonatal period—prior to the onset of synaptic stripping of motor neurons[35] and while the complement system remains underdeveloped[36] —exploiting the high-permeability window of the blood-brain barrier (BBB)[37] enables highly efficient transduction of the central nervous system (CNS) via intramuscular injection of rAAV2-retro. This facilitates comprehensive gene silencing across

spinal motor neurons. This therapeutic strategy effectively curbs the toxic accumulation of misfolded SOD1 protein, halting the downstream molecular cascade involving mitochondrial dysfunction, glial cell activation, and excitotoxicity.[38] Third, the neonatal immune system's immaturity significantly reduces adaptive immune responses against the viral capsid or transgenic products, ensuring long-term, stable expression of the transgene. Compared to the limitations of adult interventions requiring high doses or invasive procedures due to mature BBB and heightened immune surveillance, this highlights the unique advantage of early intervention in ALS gene therapy. Fourth, building upon these results, we propose a novel theoretical framework for newborn screening and preemptive intervention in high-risk *SOD1*-ALS families. This involves identifying *SOD1* mutation carriers through genetic screening and administering gene therapy during the presymptomatic phase. Early intervention is anticipated to substantially reduce the lifetime cost burden of ALS management, offering significant cost-effectiveness advantages. This developmentally timed intervention, implemented during a window of heightened neuroplasticity, transcends the traditional "post-damage repair" paradigm for neurodegenerative diseases. It provides a translatable preventive strategy for other motor neuron disorders like spinal muscular atrophy (SMA) and inherited neurological conditions.

Current delivery strategies for ALS gene therapy include intrathecal (IT), intracerebroventricular (ICV), or spinal parenchymal (SP) injections. These approaches require complex medical devices or high-risk surgical procedures, posing significant challenges for clinical translation. For example, intrathecal administration requires lumbar puncture, which may lead to complications such as post-procedural headaches, cerebrospinal fluid (CSF) leakage, and infections.[39] Furthermore, AAV vectors delivered intrathecally may activate cytotoxic T lymphocytes (CTLs), triggering neuroinflammatory responses targeting dorsal root ganglia and resulting in neuronal loss and immune cell infiltration.[39] More critically, preclinical studies indicate that achieving full spinal cord coverage via intrathecal injection necessitates large vector volumes (e.g., administering approximately half the total CSF volume in humans), a method that could induce toxicity in humans due to rapid fluctuations in intracranial pressure and electrolyte imbalances.[40] These technical and safety limitations severely restrict the clinical applicability of intrathecal injection. Compared to intrathecal delivery, intramuscular injection demonstrates distinct technical and safety advantages. As a non-invasive delivery method, intramuscular injection requires no complex medical devices or high-risk surgical procedures, significantly reducing clinical implementation challenges and complication risks. Studies have shown that intramuscular injection of rAAV vectors enables retrograde axonal transport to target spinal motor neurons, achieving efficient central nervous system (CNS) transduction while minimizing systemic exposure. For instance, in *SOD1*^{G93A} ALS mouse models, intramuscular delivery of AAV6-HGF improved muscle histology, delayed disease progression, and extended survival.[28] Similarly, intramuscular delivery of AAV9-IGF2 not only preserved motor neurons but also induced axonal regeneration.[26] These findings highlight the targeting precision, low

invasiveness, and sustained efficacy of intramuscular injection, positioning it as a highly promising delivery strategy for ALS gene therapy. Our study advances this paradigm through several key innovations. Firstly, our strategy employs a lower viral dose than typical AAV studies, reducing manufacturing costs while maintaining efficacy. Secondly, neonatal intervention at postnatal day 4 (P4) – during the very early presymptomatic stage – enables substantially earlier blockade of disease progression than most established protocols. Moreover, unlike systemic intravenous delivery requiring massive doses for partial spinal coverage, our intramuscular approach achieves potent, neuron-selective transduction of spinal motor neurons, thereby overcoming the dose limitations inherent to intravenous administration. Mechanistically, our strategy fundamentally differs from prior IM work: Previous studies primarily delivered neurotrophic factors (e.g., IGF-1, IGF-2, HGF) via IM injection to ameliorate pathology. While beneficial, these approaches offer modest efficacy due to their single-mechanism, symptomatic focus.[24-26,28]. In contrast, our study employs rAAV2-retro-mediated *SOD1* gene silencing during the neonatal period, targeting the genetic root cause of ALS. This causal intervention disrupts the disease cascade at its origin, yielding multidimensional therapeutic benefits: improved motor function, enhanced motor neuron survival, reduced apoptosis and neuroinflammation, preserved neuromuscular junctions (NMJs), and mitigated muscle pathology. The scope of this assessment exceeds that of most prior studies. Collectively, we demonstrate that genetic silencing comprehensively corrects core ALS pathologies, validating the broad efficacy of causal gene-targeting therapies.

Mutations in the superoxide dismutase 1 (*SOD1*) gene account for approximately 20% of familial amyotrophic lateral sclerosis (ALS) cases, with over 150 pathogenic variants identified to date.[41] Substantial evidence suggests that *SOD1* mutations drive ALS pathogenesis through multiple mechanisms. A prevailing hypothesis posits that mutant *SOD1* acquires toxic gain-of-function properties, leading to protein misfolding and aggregation—a histopathological hallmark of *SOD1*-mediated ALS.[42,43] Notably, *SOD1* inclusions are also implicated in sporadic ALS, suggesting that SOD1-targeted therapies may benefit a broader patient population beyond familial cases.[44,45] Although the precise mechanistic cascade remains incompletely defined, consensus exists that SOD1-mediated toxicity disrupts critical cellular functions, collectively contributing to motor neuron (MN) degeneration.[46,47] Consequently, reducing mutant SOD1 expression represents a rational therapeutic strategy. Preclinical studies demonstrate that silencing mutant *SOD1* extends survival, delays symptom onset, and preserves motor function in ALS rodent models, positioning it as a leading target for gene therapy approaches.[48] Unlike neurotrophic support strategies (e.g., IGF1, BDNF) that modulate downstream consequences of neurodegeneration, direct silencing of mutant *SOD1* addresses the primary disease driver[17]. As the first genetically defined form of ALS, *SOD1* has been extensively investigated in AAV-RNAi-based interventions, with progressive refinement of therapeutic efficacy.[49] Our study significantly advances this paradigm by establishing a translatable platform for efficient *SOD1* suppression. The

rAAV2-retro intramuscular delivery system achieves broad MN transduction in newborn animals. This strategy is readily adaptable for targeting other ALS-linked genes (e.g., *C9orf72*, *FUS*, *TARDBP*)[50] or motor neuron disease-associated mutations, offering a versatile clinical platform for MN diseases.

In this study, four artificial miRNA sequences targeting human SOD1 were delivered via rAAV2-retro by neonatal intramuscular injection, achieving effective gene silencing and therapeutic efficacy. Crucially, parallel experiments in wild-type mice revealed that rAAV2-retro-delivered shRNA constructs induced rapid weight loss and uniform lethality within three weeks post-injection, underscoring the acute toxicity of shRNA-based approaches. This stark contrast underscores the critical safety advantage of artificial miRNAs over shRNAs in CNS-directed gene therapy. Mechanistic rationale: While both utilize RISC for silencing, shRNAs (Pol III-driven, perfect complementarity) risk RNAi pathway saturation by competing for Exportin-5, leading to global microRNA dysfunction and acute toxicity—consistent with neonatal lethality observed here and previously reported.[51] Artificial miRNAs (Pol II-driven, engineered mismatches) mimic endogenous pri-miRNA processing, mitigating saturation risk while maintaining target specificity.[17] Though potential cardiotoxicity from muscle-directed RNAi cannot be excluded,[52] the rapid lethality and rAAV2-retro's neuronal tropism suggest acute neuronal RNAi dysregulation dominates. This outcome validates the superior safety profile of engineered miRNAs over shRNAs, underscoring their critical advantage for clinical translation in ALS gene therapy.

Our work establishes a foundational therapeutic strategy by demonstrating that neonatal intramuscular delivery of rAAV2-retro vectors enables preemptive silencing of pathogenic SOD1 at its genetic source, effectively delaying ALS onset and mortality in transgenic mice. This approach provides a critical platform for subsequent therapeutic reinforcement or sustained intervention. Future directions include developing dual-component vectors (e.g., co-delivering SOD1-targeting miRNA with neuroprotective factors such as IGF1) and exploring combinatorial regimens that integrate this neonatal intervention with adult-stage therapies. The pan-spinal motor neuron transduction achieved by rAAV2-retro via intramuscular injection unlocks transformative potential for spinal cord research. Beyond ALS therapy, this platform enables precise dissection of spinal circuits through Cre/loxP or CRISPR systems, facilitating targeted gene manipulation to model diseases like hereditary spastic paraplegia or spinal muscular atrophy. Integration with optogenetic (e.g., ChR2) or chemogenetic tools (e.g., DREADDs) permits real-time functional mapping of motor ensembles in locomotion and pain processing, while calcium indicators (e.g., GCaMP) bridge histological changes to functional outcomes during disease progression. Therapeutically, the strategy supports multi-target interventions—combining neuroprotective factor, gene silencer, and regenerative promoters—to combat neurodegeneration synergistically. Its minimally invasive delivery enhances clinical feasibility, and future refinements in vector tropism optimization and immune evasion, validated in large-animal models, will accelerate

translation into precision therapies for spinal disorders, advancing innovative paradigms in neuromedicine.

Figures

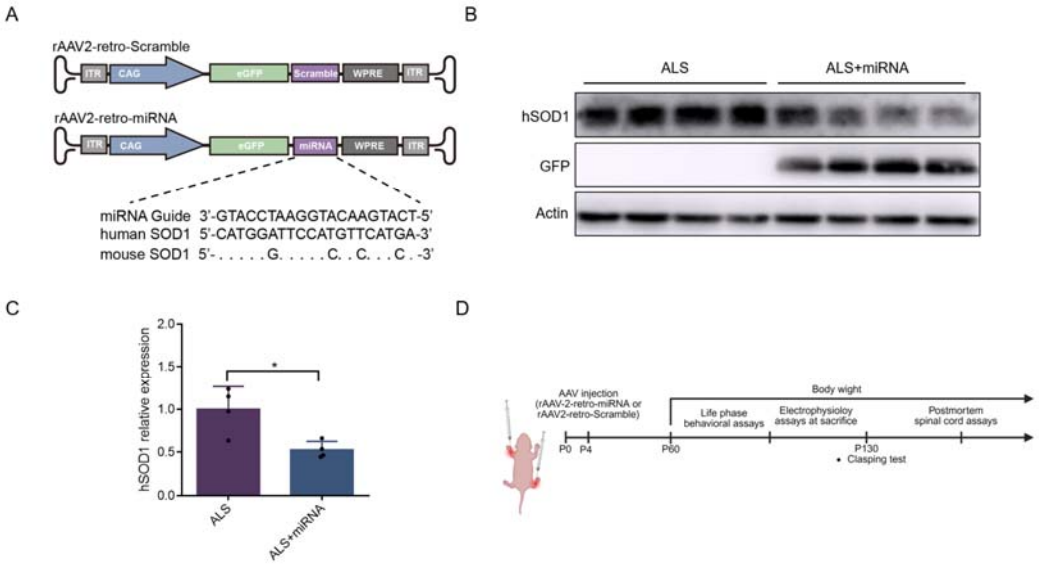

Figure 1 Design and *in vivo* validation of miRNA-hSOD1, an artificial miRNA targeting human SOD1.

(A) Schematic of the AAV vector expressing miRNA-hSOD1. The artificial miRNA was designed with perfect complementarity to human SOD1 and is based on the backbone of cellular miR-30a. A scrambled miRNA that does not target any known gene product was used as a negative control. WPRE: woodchuck hepatitis post-transcriptional regulatory element; ITR: inverted terminal repeat. (B) Western blot analysis of human SOD1 protein expression in spinal cord tissues from from WT, rAAV2-retro-Scramble-treated or rAAV2-retro-miRNA-treated ALS mice. (C) Quantification of human SOD1 suppression in spinal cord tissues. Data are presented as means ± SD, n=4 mice per group. Student's t test. *P < 0.05. (D) Schematic overview of the experimental timeline and analytical approaches used for ante-mortem and post-mortem evaluations.

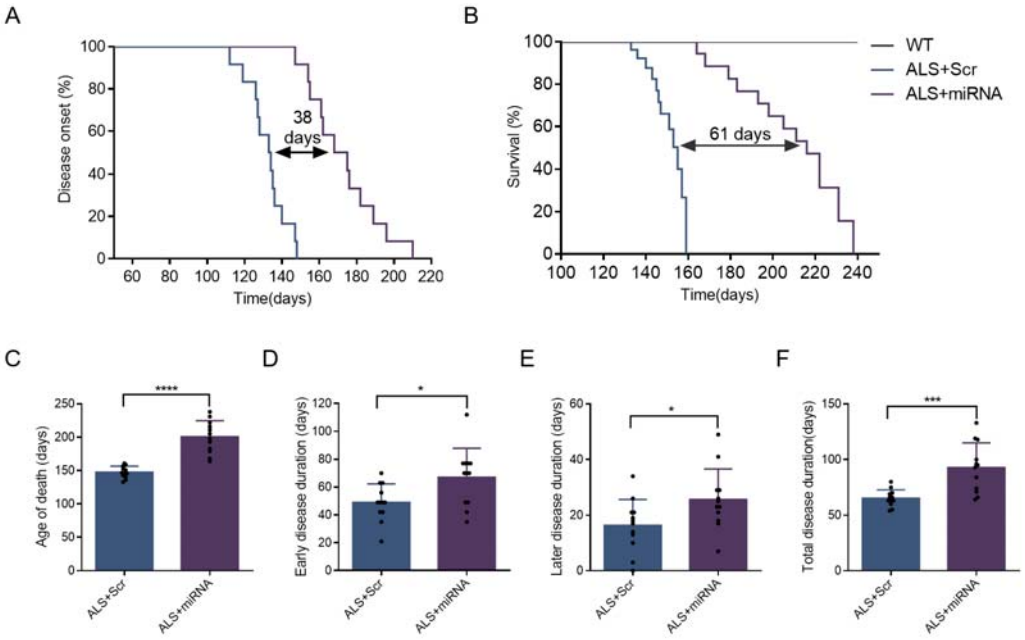

Figure 2. Intramuscular delivery of rAAV2-retro-miRNA delays paralysis, prolongs disease progression and improves survival in neonatal *SOD1*^{G93A} Mice.

(A) Kaplan-Meier curves showing disease onset, defined as a 10% decrease from peak body weight, in rAAV2-retro-miRNA-treated and rAAV2-retro-Scramble-treated *SOD1*^{G93A} mice. Differences were analyzed using the log rank (Mantel-Cox) test. (B) Kaplan-Meier survival curves of rAAV2-retro-miRNA-treated and rAAV2-retro-Scramble-treated *SOD1*^{G93A} mice. Differences were assessed with the log rank (Mantel-Cox) test. (C) Quantification of median survival in rAAV2-retro-miRNA-treated and rAAV2-retro-Scramble-treated *SOD1*^{G93A} mice. Data represent means ± SD. Student's t test. (D) Early disease duration in miRNA-treated and scramble-treated *SOD1*^{G93A} mice. Data represent means ± SD, Student's t test. (E) Disease duration in rAAV2-retro-miRNA-treated and rAAV2-retro-Scramble-treated *SOD1*^{G93A} mice. Data represent means ± SD, Student's t test. (F) Total disease duration in miRNA-treated and scramble-treated *SOD1*^{G93A} mice. Data represent means ± SD, Student's t test; n = 12 mice per group. *P < 0.05, ***P < 0.001, ****P < 0.0001.

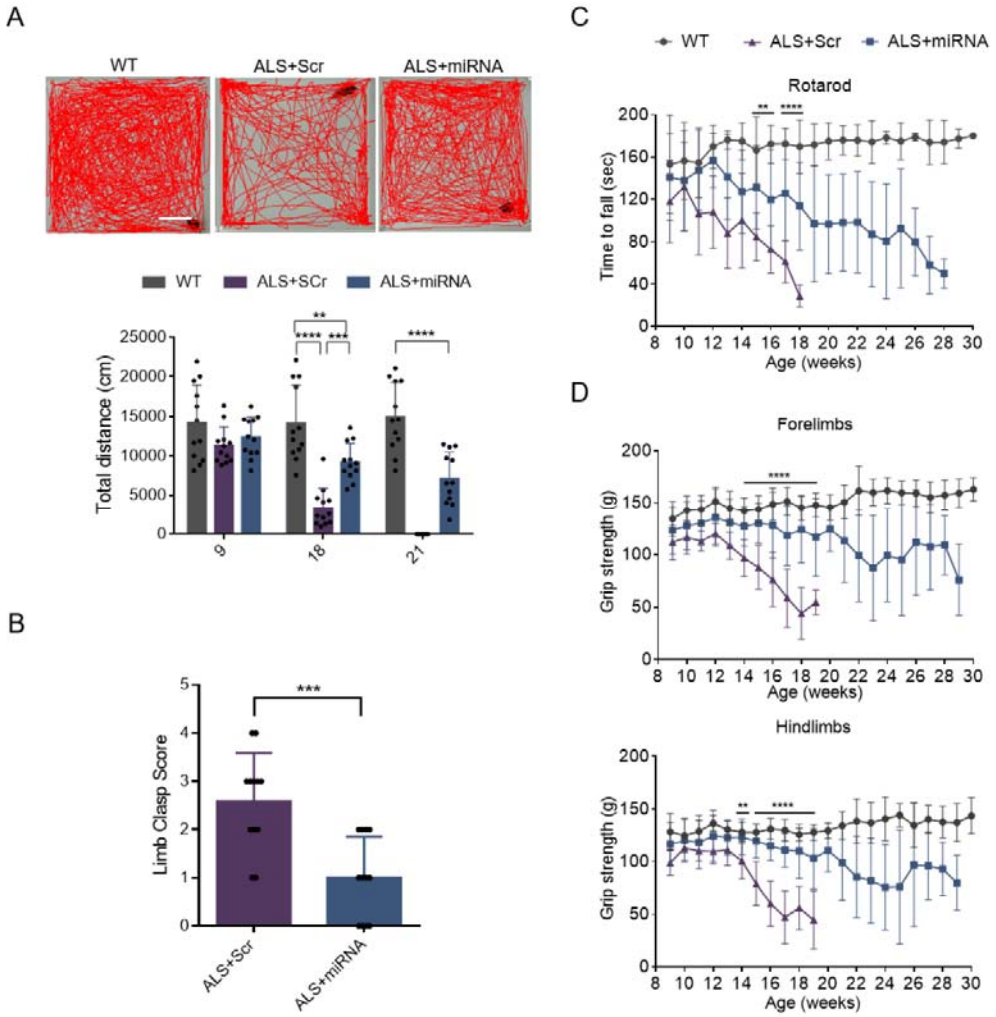

Figure 3. Intramuscular delivery of rAAV2-retro- miRNA leads to long-term preservation of motor function in neonatal *SOD1*^{G93A} Mice.

(A) Open-field motor activity, measured as total distance traveled per hour, in WT, rAAV2-retro-Scramble-treated and rAAV2-retro-miRNA-treated ALS mice. Scale bar, 10cm. ANOVA with Tukey ' s post hoc test. (B) Limb clasping score in WT, rAAV2-retro-Scramble-treated and rAAV2-retro-miRNA-treated ALS mice. Student's t test. **P < 0.01, ***P < 0.001, ****P < 0.0001. (C) Rotarod performance of WT, rAAV2-retro-Scramble-treated and rAAV2-retro-miRNA-treated ALS mice. ANOVA with Tukey's post hoc test. (D) Forelimb and hindlimb grip strength in WT, rAAV2-retro-Scramble-treated and rAAV2-retro-miRNA-treated ALS mice. ANOVA with Tukey's post hoc test. Data represent means ± SD ; n = 12 mice per group. **P < 0.01, ***P < 0.001, ****P < 0.0001 for the comparison between rAAV2-retro-Scramble-treated and rAAV2-retro-miRNA-treated groups

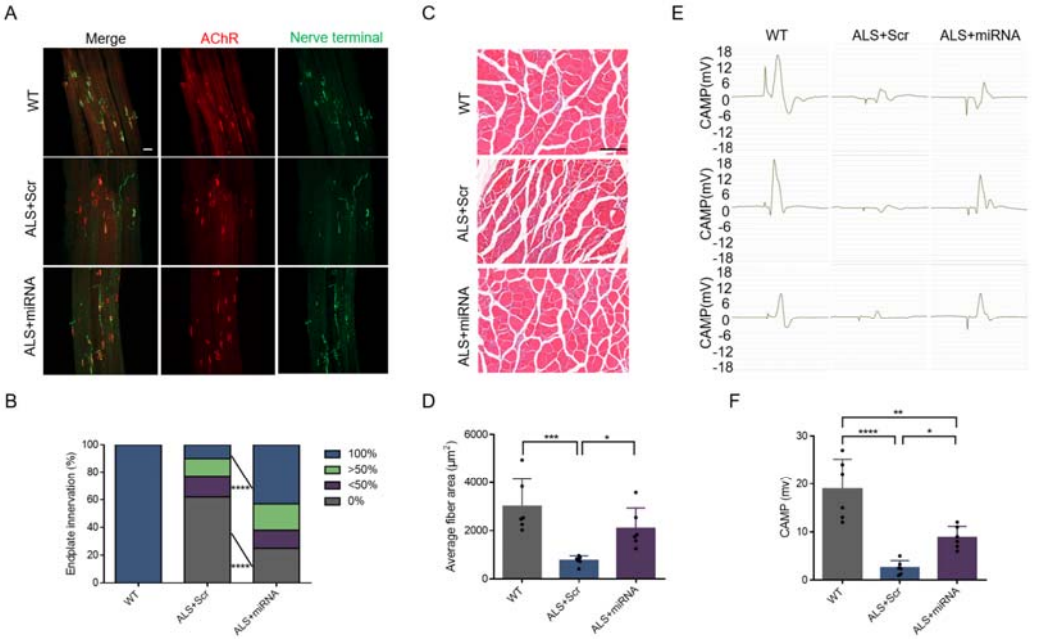

Figure 4. Intramuscular delivery of rAAV2-retro-miRNA preserves neuromuscular junctions, muscle fiber integrity, and motor function in neonatal *SOD1*^{G93A} Mice.

(A) Representative immunofluorescence images of gastrocnemius muscles from WT, rAAV2-retro-Scramble-treated or rAAV2-retro-miRNA-treated ALS mice. Sections were stained with antibodies against neurofilament (NF, presynaptic marker) and α-bungarotoxin (α-BTX, postsynaptic acetylcholine receptor marker). Scale bar, 50 μ m. (B) Quantification of neuromuscular junction (NMJ) innervation status, categorized as fully innervated (100%), partially innervated, or fully denervated (0%). Student's t test. (C) Left: Representative H&E-stained sections of gastrocnemius muscle. Scale bar: 150 μm. Right: Mean cross-sectional area (CSA) of muscle fibers. ANOVA with Tukey's post hoc test. (D) Representative compound muscle action potential (CMAP) recordings from wild-type nontransgenic (left), rAAV2-retro–Scramble-treated (middle), and rAAV2-retro-miRNA-treated *SOD1*^{G93A} mice (right). (E) Quantitative analysis of CMAP amplitudes. ANOVA with Tukey's post hoc test. Data represent mean□±□SD ,n=6 mice per group. *P < 0.05, **P < 0.01, ***P < 0.001****P < 0.0001.

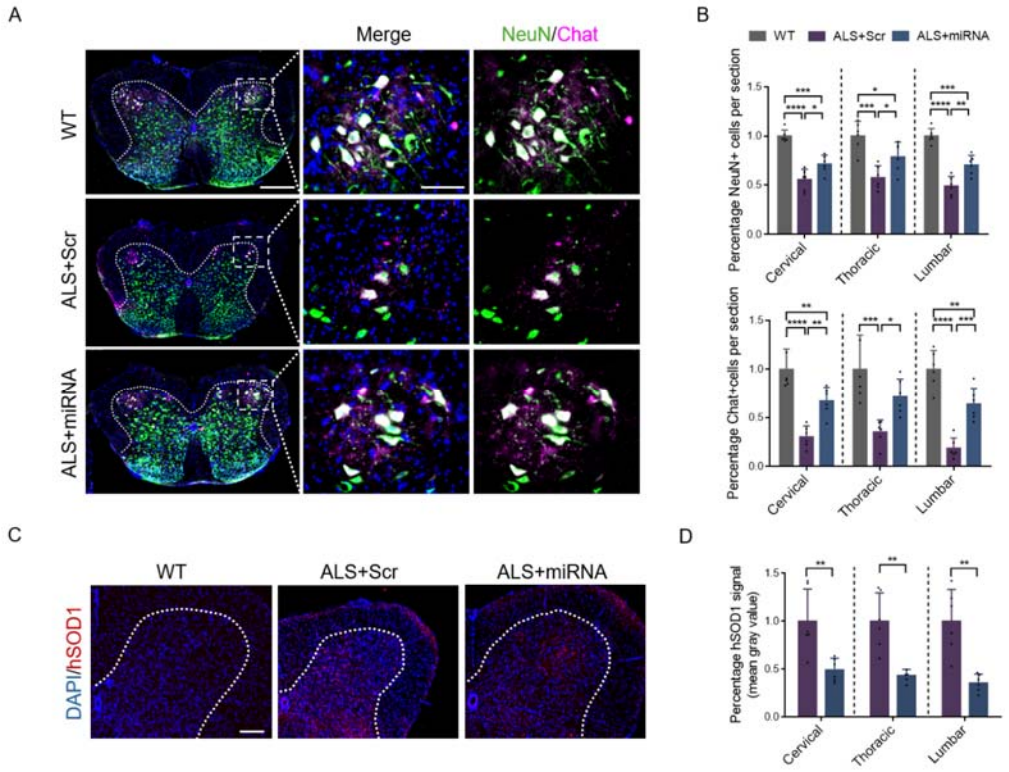

Figure 5. Intramuscular delivery of rAAV2-retro-miRNA preserves α-motor neurons and reduces SOD1 protein accumulation in *SOD1*^{G93A} Mice.

(A) Representative immunofluorescence images of lumbar spinal cord sections from WT, rAAV2-retro-Scramble-treated and rAAV2-retro-miRNA-treated ALS mice at day 130. Staining markers: NeuN (green), choline acetyltransferase (ChAT, carmine), and eGFP (gray). Nuclei are counterstained with DAPI (blue). Scale bar, 400μm(left) or 100 μm(right). (B) Quantification of α-motor neurons and NeuN□ neurons in cervical, thoracic, and lumbar spinal cord regions. ANOVA with Tukey's post hoc test. (C) Representative images of hSOD1 immunostaining in lumbar spinal cord sections from WT, rAAV2-retro-Scramble-treated and rAAV2-retro-miRNA-treated ALS mice on day 130. Nuclei are labeled with DAPI (blue); hSOD1 is shown in red. Scale bar, 200 μm. (D) Quantitative analysis of hSOD1 expression levels in cervical, thoracic, and lumbar spinal cord regions. Student's t test. Data represent mean□±□SD , n=6 mice per group. *P < 0.05, **P< 0.01, ***P < 0.001, ****P < 0.0001.

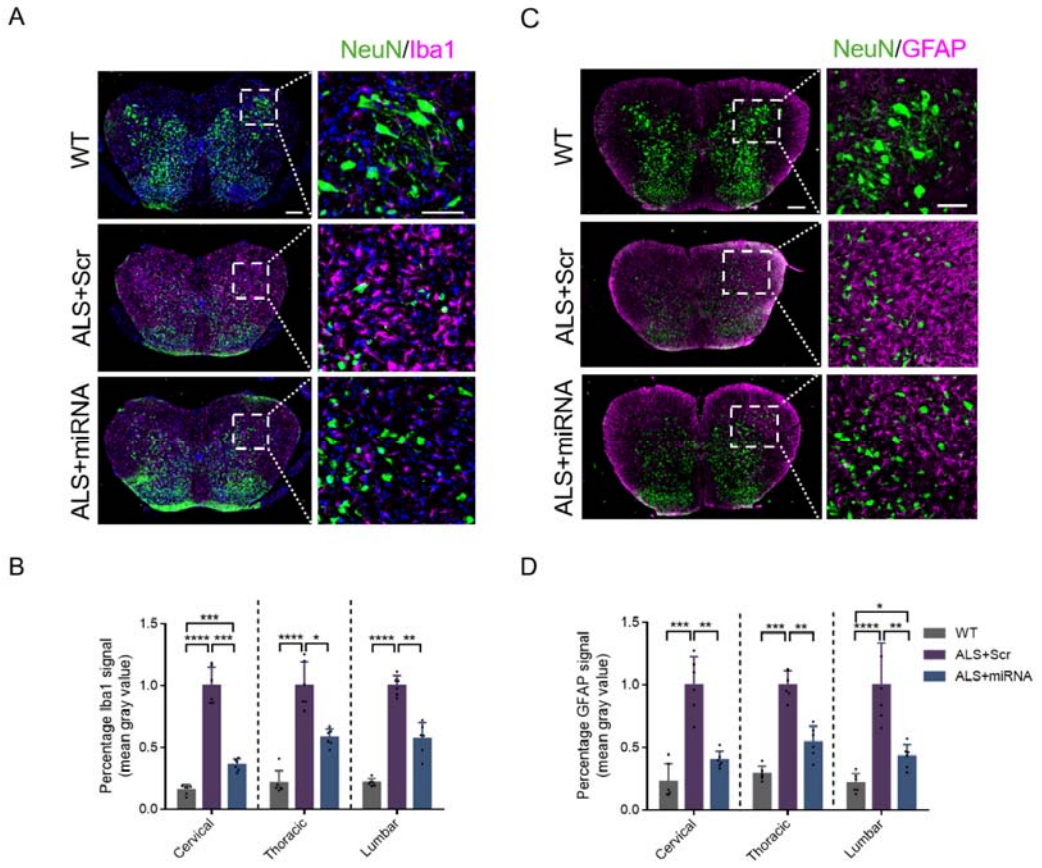

Figure 6. Intramuscular delivery of rAAV2-retro-miRNA attenuates neuroinflammation in *SOD1* ^{G93A} mice

(A) Representative immunofluorescence images of Iba1□ microglia in lumbar spinal cord sections from WT, rAAV2-retro-Scramble-treated and rAAV2-retro-miRNA-treated ALS mice. Scale bars, 200 μm (left) or 100 μm (right). (B) Quantification of Iba1 fluorescence intensity in the gray matter of wild-type (WT) and treated mice. (C) Representative immunofluorescence images of GFAP□ astrocytes in lumbar spinal cord sections from WT, rAAV2-retro-Scramble-treated and rAAV2-retro-miRNA-treated ALS mice. Scale bars, 200 μm (left) or 100 μm (right). (D) Quantification of GFAP fluorescence intensity in the gray matter. Data represent mean□±□SD，n=6 mice per group. ANOVA with Tukey's post hoc test. *P < 0.05, **P < 0.01, ***P < 0.001, ****P < 0.0001.

Supplementary figure 1：The artificial miRNA does not affect murine SOD1 mRNA expression *in vitro*.

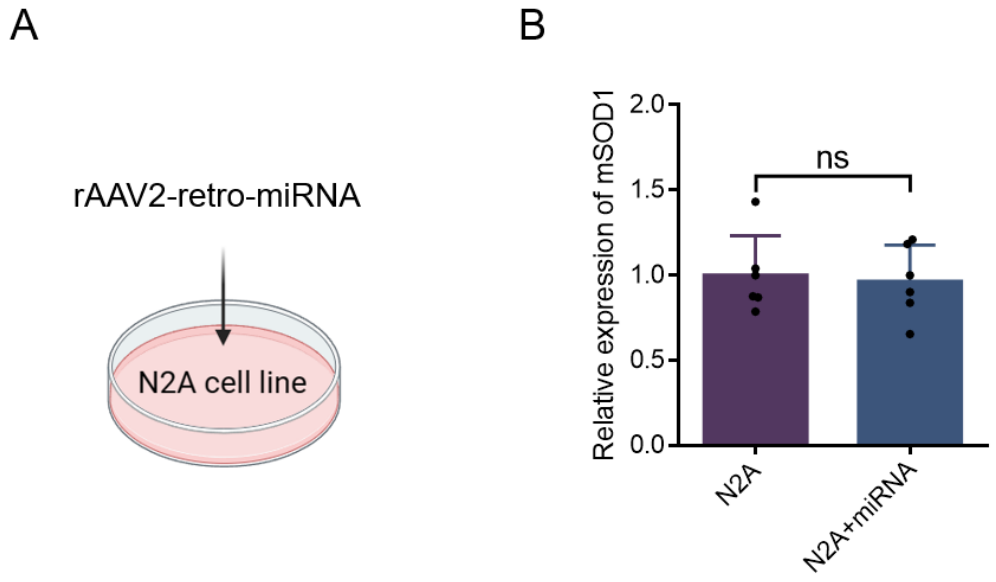

(A) N2A cells were transduced with rAAV2-retro–miRNA for 48 hours, followed by total RNA extraction.

(B) Quantification of murine SOD1 (mSOD1) mRNA levels via qPCR, normalized to mGAPDH. Data are presented as individual biological replicates (dots). ns, not significant. Data represent mean□±□SD, n=6 per group. Student's t test.

Supplementary figure 2: Comparative safety evaluation of rAAV2-retro-shRNA and rAAV2-retro-miRNA in wild-type mice.

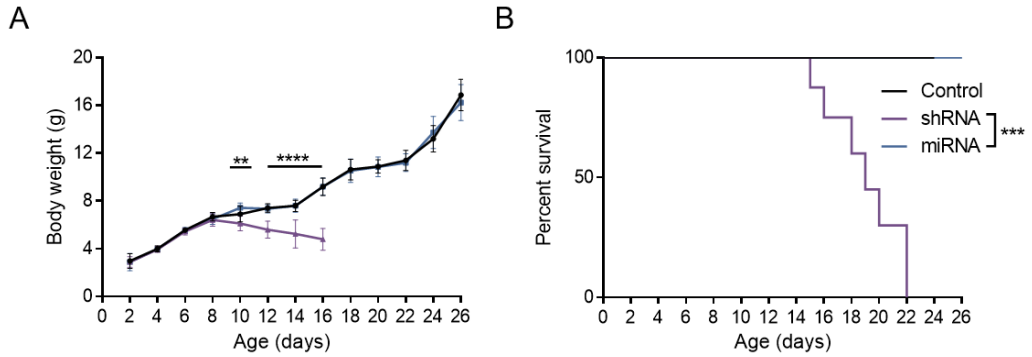

(A) Body weight curves of wild-type mice following intramuscular injection of rAAV2-retro-shRNA or rAAV2-retro-miRNA at postnatal day 4 (P4). n=6 mice per group. ANOVA with Tukey's post hoc test. **P < 0.01, ****P < 0.0001 for the comparison between rAAV2-retro-Scramble-treated and rAAV2-retro-miRNA-treated groups. (B) Kaplan–Meier survival curves of wild-type mice after injection of rAAV2-retro-shRNA or rAAV2-retro-miRNA. Differences were assessed with the log-rank (Mantel–Cox) test. Data are presented as mean ± SD, n=6 mice per group, ***P < 0.001.

Supplementary figure 3：Intramuscular delivery of rAAV2-retro attenuates weight loss in *SOD1* ^{G93A} mice

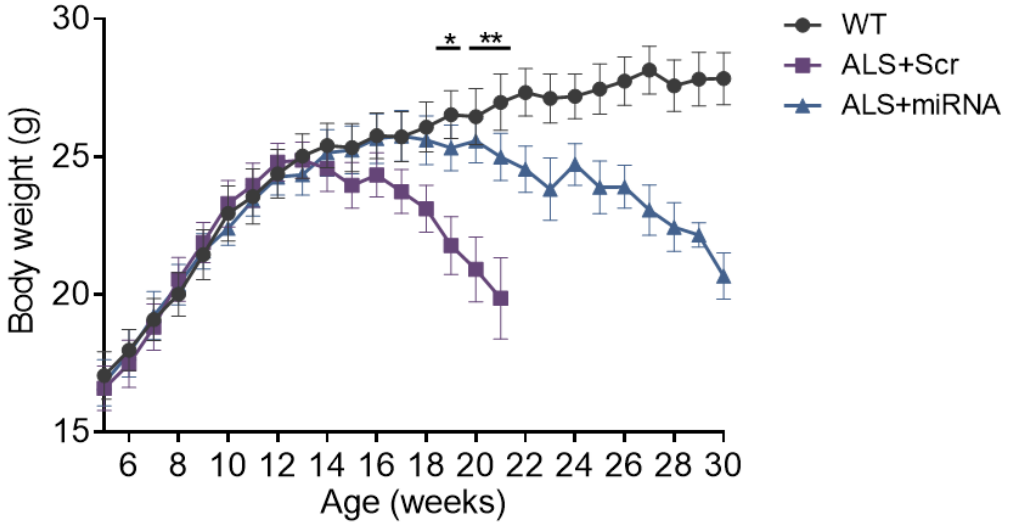

Comparison of the body weight curves of WT, rAAV2-retro-Scramble-treated and rAAV2-retro-miRNA-treated ALS mice. n=12 mice per group; ANOVA with Tukey's post hoc test. *P < 0.05, **P < 0.01 for the comparison between rAAV2-retro-Scramble-treated and rAAV2-retro-miRNA-treated groups.

Supplementary figure 4：Representative images and quantitative analysis of the gastrocnemius muscle from at day 130 WT and *SOD1*^{G93A} mice

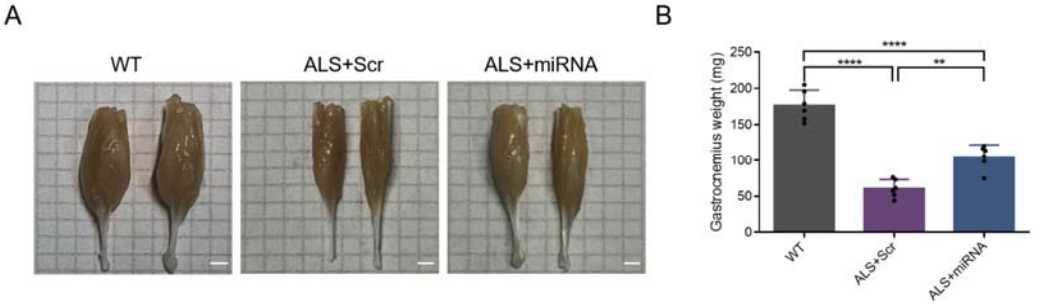

(A) Gastrocnemius muscle sections from P130 WT, rAAV2-retro-Scramble-treated and rAAV2-retro-miRNA-treated ALS mice. Scale bar, 2mm. (B) Muscle weight quantification. Data represent mean ± SD; n = 6 mice per group. **P< 0.01, ****P < 0.0001; ANOVA with Tukey's post hoc test.

ACKNOWLEDGMENTS

This work was sponsored by the Natural Science Foundation of Shanghai under Grant Nos. 22ZR1414500, 21ZR1407700 (to T.X.).

AUTHOR CONTRIBUTIONS

Conceptualization: W.W., T.X.; data curation: X.G.; supervision: W.W., T.X.; visualization: X.G., T.X.; writing-original draft: X.G., Y.X., W.W., T.X.

DECLARATION OF INTERESTS

The authors declare no competing interests.

REFERENCES

1. Siddique, N., and Siddique, T. (1993). Amyotrophic Lateral Sclerosis Overview. In GeneReviews(®), M.P. Adam, J. Feldman, G.M. Mirzaa, R.A. Pagon, S.E. Wallace, and A. Amemiya, eds. (Seattle (WA): University of Washington, SeattleCopyright © 1993-2025, University of Washington, Seattle. GeneReviews is a registered trademark of the University of Washington, Seattle. All rights reserved.).
2. Mejzini, R., Flynn, L.L., Pitout, I.L., Fletcher, S., Wilton, S.D., and Akkari, P.A. (2019). ALS Genetics, Mechanisms, and Therapeutics: Where Are We Now? Front Neurosci *13*, 1310. 10.3389/fnins.2019.01310.
3. Petrov, D., Mansfield, C., Moussy, A., and Hermine, O. (2017). ALS Clinical Trials Review: 20 Years of Failure. Are We Any Closer to Registering a New Treatment? Front Aging Neurosci *9*, 68. 10.3389/fnagi.2017.00068.
4. Sawada, H. (2017). Clinical efficacy of edaravone for the treatment of amyotrophic lateral sclerosis. Expert Opin Pharmacother *18*, 735-738. 10.1080/14656566.2017.1319937.
5. Cetin, H., Rath, J., Füzi, J., Reichardt, B., Fülöp, G., Koppi, S., Erdler, M., Ransmayr, G., Weber, J., Neumann, K., Hagmann, M., et al. (2015). Epidemiology of amyotrophic lateral sclerosis and effect of riluzole on disease course. Neuroepidemiology *44*, 6-15. 10.1159/000369813.
6. Paganoni, S., Hendrix, S., Dickson, S.P., Knowlton, N., Berry, J.D., Elliott, M.A., Maiser, S., Karam, C., Caress, J.B., Owegi, M.A., Quick, A., et al. (2022). Effect of sodium phenylbutyrate/taurursodiol on tracheostomy/ventilation-free survival and hospitalisation in amyotrophic lateral sclerosis: long-term results from the CENTAUR trial. J Neurol Neurosurg Psychiatry *93*, 871-875. 10.1136/jnnp-2022-329024.
7. Chia, R., Chiò, A., and Traynor, B.J. (2018). Novel genes associated with amyotrophic lateral sclerosis: diagnostic and clinical implications. Lancet Neurol *17*, 94-102. 10.1016/s1474-4422(17)30401-5.
8. Rosen, D.R., Siddique, T., Patterson, D., Figlewicz, D.A., Sapp, P., Hentati, A., Donaldson, D., Goto, J., O'Regan, J.P., Deng, H.X., and et al. (1993). Mutations in Cu/Zn superoxide dismutase gene are associated with familial amyotrophic lateral sclerosis. Nature *362*, 59-62. 10.1038/362059a0.
9. Arai, T., Hasegawa, M., Akiyama, H., Ikeda, K., Nonaka, T., Mori, H., Mann, D., Tsuchiya, K.,

Yoshida, M., Hashizume, Y., and Oda, T. (2006). TDP-43 is a component of ubiquitin-positive tau-negative inclusions in frontotemporal lobar degeneration and amyotrophic lateral sclerosis. Biochem Biophys Res Commun *351*, 602-611. 10.1016/j.bbrc.2006.10.093.

10. Neumann, M., Sampathu, D.M., Kwong, L.K., Truax, A.C., Micsenyi, M.C., Chou, T.T., Bruce, J., Schuck, T., Grossman, M., Clark, C.M., McCluskey, L.F., et al. (2006). Ubiquitinated TDP-43 in frontotemporal lobar degeneration and amyotrophic lateral sclerosis. Science *314*, 130-133. 10.1126/science.1134108.
11. Vance, C., Rogelj, B., Hortobágyi, T., De Vos, K.J., Nishimura, A.L., Sreedharan, J., Hu, X., Smith, B., Ruddy, D., Wright, P., Ganesalingam, J., et al. (2009). Mutations in FUS, an RNA processing protein, cause familial amyotrophic lateral sclerosis type 6. Science *323*, 1208-1211. 10.1126/science.1165942.
12. Kwiatkowski, T.J., Jr., Bosco, D.A., Leclerc, A.L., Tamrazian, E., Vanderburg, C.R., Russ, C., Davis, A., Gilchrist, J., Kasarskis, E.J., Munsat, T., Valdmanis, P., et al. (2009). Mutations in the FUS/TLS gene on chromosome 16 cause familial amyotrophic lateral sclerosis. Science *323*, 1205-1208. 10.1126/science.1166066.
13. Renton, A.E., Majounie, E., Waite, A., Simón-Sánchez, J., Rollinson, S., Gibbs, J.R., Schymick, J.C., Laaksovirta, H., van Swieten, J.C., Myllykangas, L., Kalimo, H., et al. (2011). A hexanucleotide repeat expansion in C9ORF72 is the cause of chromosome 9p21-linked ALS-FTD. Neuron *72*, 257-268. 10.1016/j.neuron.2011.09.010.
14. DeJesus-Hernandez, M., Mackenzie, I.R., Boeve, B.F., Boxer, A.L., Baker, M., Rutherford, N.J., Nicholson, A.M., Finch, N.A., Flynn, H., Adamson, J., Kouri, N., et al. (2011). Expanded GGGGCC hexanucleotide repeat in noncoding region of C9ORF72 causes chromosome 9p-linked FTD and ALS. Neuron *72*, 245-256. 10.1016/j.neuron.2011.09.011.
15. Matsumoto, A., Okada, Y., Nakamichi, M., Nakamura, M., Toyama, Y., Sobue, G., Nagai, M., Aoki, M., Itoyama, Y., and Okano, H. (2006). Disease progression of human SOD1 (G93A) transgenic ALS model rats. J Neurosci Res *83*, 119-133. 10.1002/jnr.20708.
16. Kaur, S.J., McKeown, S.R., and Rashid, S. (2016). Mutant SOD1 mediated pathogenesis of Amyotrophic Lateral Sclerosis. Gene *577*, 109-118. 10.1016/j.gene.2015.11.049.
17. van Zundert, B., and Brown, R.H., Jr. (2017). Silencing strategies for therapy of SOD1-mediated ALS. Neurosci Lett *636*, 32-39. 10.1016/j.neulet.2016.07.059.
18. Miller, T., Cudkowicz, M., Shaw, P.J., Andersen, P.M., Atassi, N., Bucelli, R.C., Genge, A., Glass, J., Ladha, S., Ludolph, A.L., Maragakis, N.J., et al. (2020). Phase 1-2 Trial of Antisense Oligonucleotide Tofersen for SOD1 ALS. N Engl J Med *383*, 109-119. 10.1056/NEJMoa2003715.
19. Blair, H.A. (2023). Tofersen: First Approval. Drugs *83*, 1039-1043. 10.1007/s40265-023-01904-6.
20. Rocco, M.T., Akhter, A.S., Ehrlich, D.J., Scott, G.C., Lungu, C., Munjal, V., Aquino, A., Lonser, R.R., Fiandaca, M.S., Hallett, M., Heiss, J.D., et al. (2022). Long-term safety of MRI-guided administration of AAV2-GDNF and gadoteridol in the putamen of individuals with Parkinson's disease. Mol Ther *30*, 3632-3638. 10.1016/j.ymthe.2022.08.003.
21. Ling, Q., Herstine, J.A., Bradbury, A., and Gray, S.J. (2023). AAV-based in vivo gene therapy for neurological disorders. Nat Rev Drug Discov *22*, 789-806. 10.1038/s41573-023-00766-7.
22. Boudreau, R.L., Martins, I., and Davidson, B.L. (2009). Artificial microRNAs as siRNA shuttles: improved safety as compared to shRNAs in vitro and in vivo. Mol Ther *17*, 169-175.

10.1038/mt.2008.231.

23. McBride, J.L., Boudreau, R.L., Harper, S.Q., Staber, P.D., Monteys, A.M., Martins, I., Gilmore, B.L., Burstein, H., Peluso, R.W., Polisky, B., Carter, B.J., et al. (2008). Artificial miRNAs mitigate shRNA-mediated toxicity in the brain: implications for the therapeutic development of RNAi. Proc Natl Acad Sci U S A *105*, 5868-5873. 10.1073/pnas.0801775105.
24. Kaspar, B.K., Lladó, J., Sherkat, N., Rothstein, J.D., and Gage, F.H. (2003). Retrograde viral delivery of IGF-1 prolongs survival in a mouse ALS model. Science *301*, 839-842. 10.1126/science.1086137.
25. Kaspar, B.K., Frost, L.M., Christian, L., Umapathi, P., and Gage, F.H. (2005). Synergy of insulin-like growth factor-1 and exercise in amyotrophic lateral sclerosis. Ann Neurol *57*, 649-655. 10.1002/ana.20451.
26. Allodi, I., Comley, L., Nichterwitz, S., Nizzardo, M., Simone, C., Benitez, J.A., Cao, M., Corti, S., and Hedlund, E. (2016). Differential neuronal vulnerability identifies IGF-2 as a protective factor in ALS. Sci Rep *6*, 25960. 10.1038/srep25960.
27. Lin, H., Hu, H., Duan, W., Liu, Y., Tan, G., Li, Z., Liu, Y., Deng, B., Song, X., Wang, W., Wen, D., et al. (2018). Intramuscular Delivery of scAAV9-hIGF1 Prolongs Survival in the hSOD1(G93A) ALS Mouse Model via Upregulation of D-Amino Acid Oxidase. Mol Neurobiol *55*, 682-695. 10.1007/s12035-016-0335-z.
28. Lee, S.H., Lee, N., Kim, S., Lee, J., Choi, W., Yu, S.S., Kim, J.H., and Kim, S. (2019). Intramuscular delivery of HGF-expressing recombinant AAV improves muscle integrity and alleviates neurological symptoms in the nerve crush and SOD1-G93A transgenic mouse models. Biochem Biophys Res Commun *517*, 452-457. 10.1016/j.bbrc.2019.07.105.
29. Chen, Z., Fan, G., Li, A., Yuan, J., and Xu, T. (2020). rAAV2-Retro Enables Extensive and High-Efficient Transduction of Lower Motor Neurons following Intramuscular Injection. Mol Ther Methods Clin Dev *17*, 21-33. 10.1016/j.omtm.2019.11.006.
30. Gurney, M.E., Pu, H., Chiu, A.Y., Dal Canto, M.C., Polchow, C.Y., Alexander, D.D., Caliendo, J., Hentati, A., Kwon, Y.W., Deng, H.X., and et al. (1994). Motor neuron degeneration in mice that express a human Cu,Zn superoxide dismutase mutation. Science *264*, 1772-1775. 10.1126/science.8209258.
31. Cheng, W., Huang, J., Fu, X.Q., Tian, W.Y., Zeng, P.M., Li, Y., and Luo, Z.G. (2023). Intrathecal delivery of AAV-NDNF ameliorates disease progression of ALS mice. Mol Ther *31*, 3277-3289. 10.1016/j.ymthe.2023.09.018.
32. Chen, S.K., Hawley, Z.C.E., Zavodszky, M.I., Hana, S., Ferretti, D., Grubor, B., Hawes, M., Xu, S., Hamann, S., Marsh, G., Cullen, P., et al. (2023). Efficacy and safety of a SOD1-targeting artificial miRNA delivered by AAV9 in mice are impacted by miRNA scaffold selection. Mol Ther Nucleic Acids *34*, 102057. 10.1016/j.omtn.2023.102057.
33. Biferi, M.G., Cohen-Tannoudji, M., Cappelletto, A., Giroux, B., Roda, M., Astord, S., Marais, T., Bos, C., Voit, T., Ferry, A., and Barkats, M. (2017). A New AAV10-U7-Mediated Gene Therapy Prolongs Survival and Restores Function in an ALS Mouse Model. Mol Ther *25*, 2038-2052. 10.1016/j.ymthe.2017.05.017.
34. Eisen, A., Kiernan, M., Mitsumoto, H., and Swash, M. (2014). Amyotrophic lateral sclerosis: a long preclinical period? J Neurol Neurosurg Psychiatry *85*, 1232-1238. 10.1136/jnnp-2013-307135.
35. Salvany, S., Casanovas, A., Piedrafita, L., Tarabal, O., Hernández, S., Calderó, J., and

Esquerda, J.E. (2021). Microglial recruitment and mechanisms involved in the disruption of afferent synaptic terminals on spinal cord motor neurons after acute peripheral nerve injury. Glia *69*, 1216-1240. 10.1002/glia.23959.

36. Yu, J.C., Khodadadi, H., Malik, A., Davidson, B., Salles É, D.S.L., Bhatia, J., Hale, V.L., and Baban, B. (2018). Innate Immunity of Neonates and Infants. Front Immunol *9*, 1759. 10.3389/fimmu.2018.01759.
37. Foust, K.D., Nurre, E., Montgomery, C.L., Hernandez, A., Chan, C.M., and Kaspar, B.K. (2009). Intravascular AAV9 preferentially targets neonatal neurons and adult astrocytes. Nat Biotechnol *27*, 59-65. 10.1038/nbt.1515.
38. Peggion, C., Scalcon, V., Massimino, M.L., Nies, K., Lopreiato, R., Rigobello, M.P., and Bertoli, A. (2022). SOD1 in ALS: Taking Stock in Pathogenic Mechanisms and the Role of Glial and Muscle Cells. Antioxidants (Basel) *11*. 10.3390/antiox11040614.
39. Meijboom, K.E., and Brown, R.H. (2022). Approaches to Gene Modulation Therapy for ALS. Neurotherapeutics *19*, 1159-1179. 10.1007/s13311-022-01285-w.
40. Hinderer, C., Katz, N., Dyer, C., Goode, T., Johansson, J., Bell, P., Richman, L., Buza, E., and Wilson, J.M. (2020). Translational Feasibility of Lumbar Puncture for Intrathecal AAV Administration. Mol Ther Methods Clin Dev *17*, 969-974. 10.1016/j.omtm.2020.04.012.
41. Tortelli, R., Conforti, F.L., Cortese, R., D'Errico, E., Distaso, E., Mazzei, R., Ungaro, C., Magariello, A., Gambardella, A., Logroscino, G., and Simone, I.L. (2013). Amyotrophic lateral sclerosis: a new missense mutation in the SOD1 gene. Neurobiol Aging *34*, 1709.e1703-1705. 10.1016/j.neurobiolaging.2012.10.027.
42. Chattopadhyay, M., and Valentine, J.S. (2009). Aggregation of copper-zinc superoxide dismutase in familial and sporadic ALS. Antioxid Redox Signal *11*, 1603-1614. 10.1089/ars.2009.2536.
43. Paré, B., Lehmann, M., Beaudin, M., Nordström, U., Saikali, S., Julien, J.P., Gilthorpe, J.D., Marklund, S.L., Cashman, N.R., Andersen, P.M., Forsberg, K., et al. (2018). Misfolded SOD1 pathology in sporadic Amyotrophic Lateral Sclerosis. Sci Rep *8*, 14223. 10.1038/s41598-018-31773-z.
44. Berdyński, M., Miszta, P., Safranow, K., Andersen, P.M., Morita, M., Filipek, S., Żekanowski, C., and Kuźma-Kozakiewicz, M. (2022). SOD1 mutations associated with amyotrophic lateral sclerosis analysis of variant severity. Sci Rep *12*, 103. 10.1038/s41598-021-03891-8.
45. Baird, M.C., Likhite, S.B., Vetter, T.A., Caporale, J.R., Girard, H.B., Roussel, F.S., Howard, A.E., Schwartz, M.K., Reed, A.R., Kaleem, A., Zhang, X., et al. (2024). Combination AAV therapy with galectin-1 and SOD1 downregulation demonstrates superior therapeutic effect in a severe ALS mouse model. Mol Ther Methods Clin Dev *32*, 101312. 10.1016/j.omtm.2024.101312.
46. Rothstein, J.D. (2009). Current hypotheses for the underlying biology of amyotrophic lateral sclerosis. Ann Neurol *65 Suppl 1*, S3-9. 10.1002/ana.21543.
47. Saccon, R.A., Bunton-Stasyshyn, R.K., Fisher, E.M., and Fratta, P. (2013). Is SOD1 loss of function involved in amyotrophic lateral sclerosis? Brain *136*, 2342-2358. 10.1093/brain/awt097.
48. Amado, D.A., and Davidson, B.L. (2021). Gene therapy for ALS: A review. Mol Ther *29*, 3345-3358. 10.1016/j.ymthe.2021.04.008.
49. Abati, E., Bresolin, N., Comi, G., and Corti, S. (2020). Silence superoxide dismutase 1

(SOD1): a promising therapeutic target for amyotrophic lateral sclerosis (ALS). Expert Opin Ther Targets *24*, 295-310. 10.1080/14728222.2020.1738390.

50. Shiryaeva, O., Tolochko, C., Alekseeva, T., and Dyachuk, V. (2025). Targets and Gene Therapy of ALS (Part 1). Int J Mol Sci *26*. 10.3390/ijms26094063.

51. Grimm, D., Streetz, K.L., Jopling, C.L., Storm, T.A., Pandey, K., Davis, C.R., Marion, P., Salazar, F., and Kay, M.A. (2006). Fatality in mice due to oversaturation of cellular microRNA/short hairpin RNA pathways. Nature *441*, 537-541. 10.1038/nature04791.

52. Course, M.M., Gudsnuk, K., Desai, N., Chamberlain, J.R., and Valdmanis, P.N. (2020). Endogenous MicroRNA Competition as a Mechanism of shRNA-Induced Cardiotoxicity. Mol Ther Nucleic Acids *19*, 572-580. 10.1016/j.omtn.2019.12.007.